Inorganic Chemistry

ARTICLE

pubs.acs.org/IC

Rational Construction of 3D Pillared Metal−Organic Frameworks: Synthesis, Structures, and Hydrogen Adsorption Properties

Ze Chang, Da-Shuai Zhang, Qiang Chen, Rui-Fang Li, Tong-Liang Hu, and Xian-He Bu*

Department of Chemistry, and Tianjin Key Lab on Metal and Molecule-Based Material Chemistry, Nankai University, Tianjin 300071, China

Supporting Information

ABSTRACT: In our efforts toward rational design and systematic synthesis of 'pillar−layer' structure MOFs, three porous MOFs have been constructed based on $[Zn_4(bpta)_2(H_2O)_2]$ (H_4bpta = 1,1′-biphenyl-2,2′,6,6′-tetracarboxylic acid) layers and three different bipyridine pillar ligands. The resulted MOFs show similar structures but different pore volume and window size depending on the length of pillar ligands which resulted in distinct gas adsorption properties. In the three MOFs, $[Zn_4(bpta)_2(4,4'\text{-bipy})_2(H_2O)_2]\cdot(DMF)_3\cdot H_2O$ (**1**) (DMF = *N*, *N*′-dimethylformamide and 4,4′-bipy = 4,4′-bipyridine) reveals selective adsorption of H_2 over N_2 and O_2 as the result of narrow pore size. $[Zn_4(bpta)_2(azpy)_2(H_2O)_2]\cdot(DMF)_4\cdot(H_2O)_3$ (**2**) and $[Zn_4(bpta)_2(dipytz)_2(H_2O)_2]\cdot(DMF)_4\cdot H_2O$ (**3**) (azpy =4,4′-azopyridine, dipytz = di-3,6-(4-pyridyl)-1,2,4,5-tetrazine) reveal pore structure change upon different activation conditions. In addition, the samples activated under different conditions show distinct adsorption behaviors of N_2 and O_2 gases. Furthermore, hydrogen adsorption properties of activated **1**−**3** were studied. The results indicated that the activation process could affect the hydrogen enthalpy of adsorption.

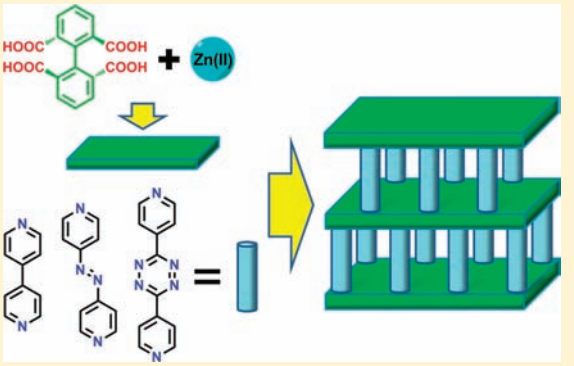

INTRODUCTION

In recent years, porous metal−organic frameworks (MOFs) have been emerging as very promising materials for gas storage, separation, heterogeneous catalysis, sensing, and drug delivery.[1] One of the most attractive targets of the research in this field is the controllable assembly of MOFs with desired structures and properties, and many strategies have already been developed.[1d,2] Among the strategies to construct porous MOFs, the 'pillar−layer' method is one of the most effective ways to synthesize new structures. In this way, the structures of a wide variety of MOFs can be predicted and the pore size and chemical functionality of the resultant open frameworks such as hydrophilic/hydrophobic character, hydrogen bonding, and open metal site can be readily controlled via modification of the pillars.[3] Also, pillar−layer systems allow postmodification without a network rearrangement and maintain the network topology when the ligand and/or conditions of synthesis are varied. This character is desired for the sake of property screening and simplified analysis of the materials.[4]

In our efforts toward rational design and systematic synthesis of pillar−layer structure MOFs, we found that multicarboxylic acids are good ligands for construction of layer structures.[5] However, formation of specific structures was not guaranteed even using similar ligands under identical conditions of synthesis as many factors can affect the structures of the final products.[6] To ensure formation of robust layer structures and further pillar−layer MOFs, we used 1,1′-biphenyl-2,2′,6,6′-tetracarboxylic acid (H_4bpta) in our studies. We found that this ligand is effective in forming robust layer structure due to its coordination with Zn(II) ions, and the layer structure could be extended by bipyridine ligands to form 3D pillar−layer porous MOFs. Herein, we report the systemic construction of a series of pillar−layer Zn(II) MOFs constructed with H_4bpta and different pillar ligands, namely, $[Zn_4(bpta)_2(4,4'\text{-bipy})_2(H_2O)_2]\cdot(DMF)_3\cdot H_2O$ (**1**), $[Zn_4(bpta)_2(azpy)_2(H_2O)_2]\cdot(DMF)_4\cdot(H_2O)_3$ (**2**), and $[Zn_4(bpta)_2(dipytz)_2(H_2O)_2]\cdot(DMF)_4\cdot H_2O$ (**3**) (DMF = *N*, *N*′-dimethylformamide, 4,4′-bipy = 4,4′-bipyridine, azpy = 4,4′-azopyridine, and dipytz = di-3,6-(4-pyridyl)-1,2,4,5-tetrazine) (see Chart 1). The resulted porous MOFs show tunable pore size depending on the length of pillar ligands which were characterized by N_2 and O_2 adsorptions. Furthermore, The H_2 storage capacities of resulted MOFs have also been characterized.

EXPERIMENTAL SECTION

Materials and General Methods. All solvents and reagents for synthesis were obtained commercially and used as received. H_4bpta,[7] azpy,[8] and dipytz[9] were synthesized according to the reported methods. IR spectra were measured on a TENSOR 27 OPUS (Bruker) FT-IR spectrometer using KBr disks dispersed with sample powders in the 4000−400 cm^{-1} range. Elemental analyses (C, H, and N) were performed on a Perkin-Elmer 240C analyzer. Thermogravimetric

Received: March 4, 2011
Published: July 21, 2011

   dx.doi.org/10.1021/ic2004485 | *Inorg. Chem.* 2011, 50, 7555–7562

Chart 1

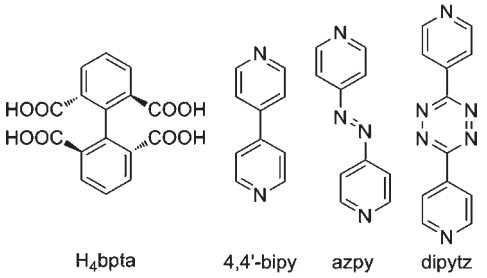

H_4bpta 4,4'-bipy azpy dipytz

analyses (TGA) were carried out on a Rigaku standard TG-DTA analyzer with a heating rate of 10 °C min^{-1} from ambient temperature to 800 °C; an empty Al_2O_3 crucible was used as reference. The room-temperature X-ray powder diffraction spectra (XRPD) were recorded on a Rigaku D/Max-2500 diffractometer at 40 kV, 100 mA with a Cu-target tube and a graphite monochromator. The variable-temperature X-ray powder diffraction was recorded with a Panalytical X'pert PRO diffractometer at 40 kV, 30 mA with a Cu-target tube and a graphite monochromator. Simulation of the XRPD pattern was carried out by the single-crystal data and diffraction-crystal module of the Mercury (Hg) program available free of charge via the Internet at http://www.iucr.org.

Synthesis of $[Zn_4(bpta)_2(4,4'\text{-bipy})_2(H_2O)_2]\cdot(DMF)_3\cdot H_2O$ (1). $Zn(NO_3)_2\cdot 6H_2O$ (0.1 mmol) was added to 12 mL of a 1:1 (v/v) mixture of DMF/ethanol containing 4,4′-bipy (0.05 mmol) and H_4bpta (0.05 mmol) under stirring in a vial, which was then sealed and allowed to stand at 100 °C for 24 h. Homogeneous colorless crystals formed were collected by filtration, washed with DMF, and dried in air (yield 60% based on H_4bpta). FT-IR (KBr pellets, cm^{-1}): 3379w, 3045w, 2929w, 1665s, 1616s, 1574s, 1553s, 1424m, 1374s, 1018m, 821m, 769m, 708m, 516w, 454w. Anal. Calcd for $C_{61}H_{55}N_7O_{22}Zn_4$: C, 48.85; H, 3.70; N, 6.54. Found: C, 48.52; H, 3.11; N, 6.63.

Synthesis of $[Zn_4(bpta)_2(azpy)_2(H_2O)_2]\cdot(DMF)_4\cdot(H_2O)_3$ (2). $Zn(NO_3)_2\cdot 6H_2O$ (0.1 mmol) was added to 12 mL of a 1:1 (v/v) mixture of DMF/ethanol containing azpy (0.05 mmol) and H_4bpta (0.05 mmol) under stirring in a vial, which was then sealed and allowed to stand at 100 °C for 24 h. Orange block crystals formed were collected by filtration, washed with DMF, and dried in air (yield 65% based on H_4bpta). FT-IR (KBr pellets, cm^{-1}): 3394w, 3103w, 1674s, 1604s, 1552s, 1456s, 1382s, 1092w, 1054w, 1028w, 840m, 776m, 713s, 662w, 569w, 450w. Anal. Calcd for $C_{64}H_{66}N_{12}O_{25}Zn_4$: C, 46.17; H, 4.00; N, 10.10. Found: C, 45.47; H, 3.71; N, 9.88.

Synthesis of $[Zn_4(bpta)_2(dipytz)_2(H_2O)_2]\cdot(DMF)_4\cdot H_2O$ (3). $Zn(NO_3)_2\cdot 6H_2O$ (0.1 mmol) was added to 10 mL of a 1:1 (v/v) mixture of DMF/ethanol containing dipytz (0.05 mmol) and H_4bpta (0.05 mmol) under stirring in a vial, which was then sealed and allowed to stand at 100 °C for 24 h. Red crystalline powder formed was collected by filtration, washed with DMF, and dried in air (yield 70% based on H_4bpta). FT-IR (KBr pellets, cm^{-1}): 3429w, 3059w, 2929w, 1669s, 1551s, 1456m, 1387s, 1152w, 1094w, 1027w, 924w, 840m, 774m, 714s, 661w, 602s, 539w, 440w. Anal. Calcd for $C_{68}H_{62}N_{16}O_{23}Zn_4$: C, 47.13; H, 3.61; N, 12.93. Found: C, 47.31; H, 3.30; N, 12.90.

X-ray Crystallography. Single-crystal X-ray diffraction measurement for **1** was carried out on a Rigaku Saturn724+ diffractometer at 113 K, and diffraction data for **2** was collected on a Rigaku Saturn70 diffractometer at 113 K. The determinations of unit cell parameters and data collections were performed with Mo Kα radiation (λ = 0.71073 Å), and unit cell dimensions were obtained with least-squares refinements. The program SAINT[10] was used for integration of the diffraction profiles. Semiempirical absorption corrections were applied using the SADABS program. The structure was solved by direct methods using the SHELXS program of the SHELXTL package and refined with SHELXL.[11] Zinc atoms were found from *E* maps, and other non-hydrogen atoms were located in successive difference Fourier syntheses. The final refinement was performed by full matrix least-squares methods with anisotropic thermal parameters for non-hydrogen atoms on F^2. The hydrogen atoms were added theoretically, riding on the concerned atoms, and refined with fixed thermal factor except for H_2O molecules. For **1**, part of the solvent DMF molecules in the compound was disordered. The disorder was treated by performing split and occupancies refinement of the disordered atoms. Part of the solvent molecules in **2** was refined with isotropic thermal parameters together with the hydrogen atoms ride on. Crystallographic data and refinement parameters are listed in Table 1.

Table 1. Crystal Data and Structure Refinement Parameters for Complexes 1 and 2

	1	2
empirical formula	$C_{61}H_{55}N_7O_{22}Zn_4$	$C_{64}H_{66}N_{12}O_{25}Zn_4$
formula weight	1499.76	1664.77
temperature/K	113	113
cryst syst	monoclinic	monoclinic
space group	*C*2/*c*	*C*2/*c*
a /Å	25.677(10)	29.943(6)
b /Å	13.996(5)	13.921(3)
c /Å	19.119(8)	18.994(4)
β /deg	118.458(5)	115.81(3)
V (Å^3)	6041(4)	7128(3)
Z	4	4
D_c (g·cm^{-3})	1.630	1.551
F(000)	3022	3416
θ range /deg	1.7−27.8	1.6−27.1
reflns collected	25154	26845
independent reflns	7159	7783
goodness-of-fit	1.24	1.10
$R_1{}^a$ ($I > 2\sigma(I)$)	0.1078	0.1272
$wR_2{}^b$ ($I > 2\sigma(I)$)	0.2085	0.3410

$^a R_1 = \Sigma||F_o| - |F_c||/\Sigma|F_o|$. $^b wR_2 = [\Sigma[w(F_o{}^2 - F_c{}^2)^2]/\Sigma w(F_o{}^2)^2]^{1/2}$.

Sorption Measurements. Gas adsorption measurements were performed using an ASAP 2020 M gas adsorption analyzer. UHP-grade gases were used in measurements. The N_2 and O_2 isotherm measurements were proceeded at 77 K in a liquid nitrogen bath. The hydrogen sorption isotherms were collected at 77 K in a liquid nitrogen bath and 87 K in a liquid argon bath.

Before measurements, the samples were soaked in methanol for 3 days to remove DMF and H_2O solvates and then filtrated and dried at room temperature. The dry samples were loaded in sample tubes and activated under high vacuum (less than 10^{-5} Torr) at different temperatures. About 85−90 mg of degassed samples was used for gas sorption measurements, and the weight of each sample was recorded before and after outgassing to confirm removal of guest molecules. The outgassing procedure was repeated on the same sample between experiments for 0.5−1 h.

RESULTS AND DISCUSSION

Syntheses and Crystal Structures. Solvothermal reactions of $Zn(NO_3)_2\cdot 6H_2O$ with H_4bpta and different bipyridine ligand in DMF/ethanol resulted in pillar−layer structure porous MOFs. For 4,4′-bipy (**1**) and azpy (**2**), the reactions offered block crystal suitable for single-crystal X-ray diffraction measurements. However, reaction with dipytz (**3**) only yields crystalline powder; then

dx.doi.org/10.1021/ic2004485 |*Inorg. Chem.* 2011, 50, 7555–7562

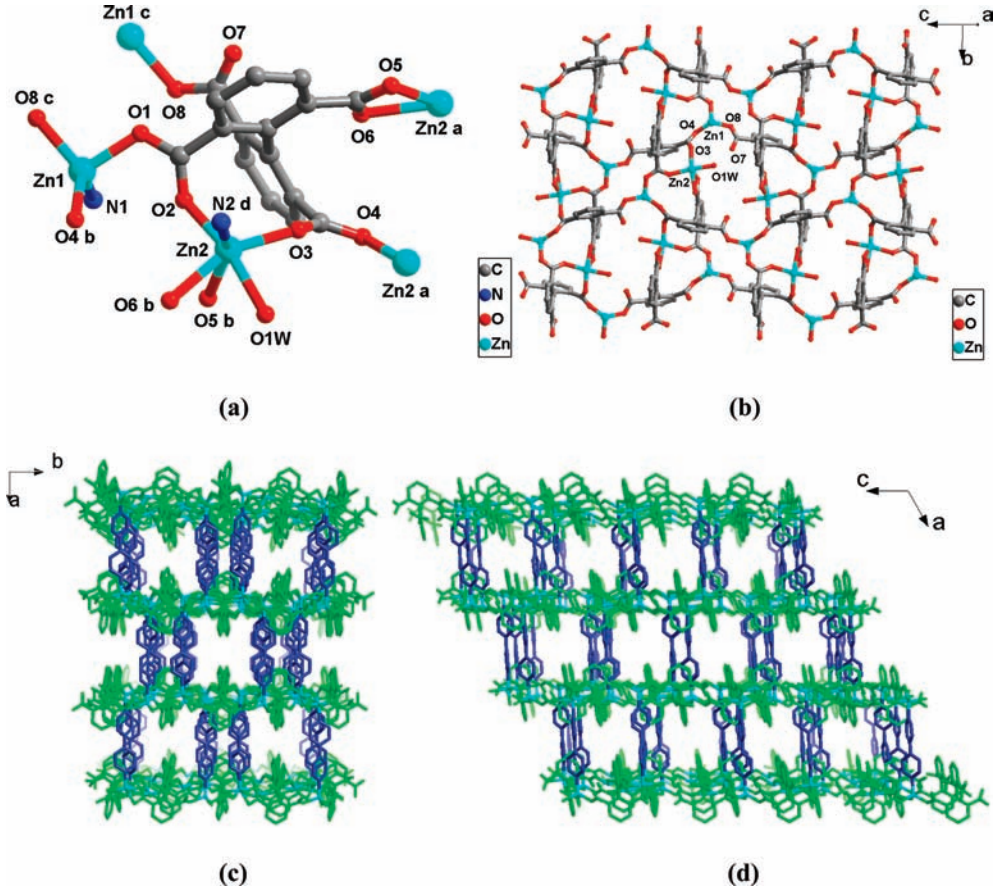

Figure 1. Crystal structure of **1**: (a) coordination environment of Zn(II) ions and $bpta^{4-}$ ligand in **1**. Symmetry codes: a, $1/2 - x, -1/2 + y, 1/2 - z$; b, $1/2 - x, 1/2 + y, 1/2 - z$; c, $1/2 - x, 1/2 - y, -z$; d, $1/2 + x, 1/2 - y, 1/2 + z$; (b) view of the 2D layer assembled by Zn(II) ions and $bpta^{4-}$ ligands. (c) views in parallel with the channels along the *c* direction; (d) views in parallel with the channels along the *b* direction.

the structure and component of product was determined by XRPD and elemental analysis.

Single-crystal structure analysis reveals that **1** crystallizes in the monoclinic system *C*2/*c* space group. As shown in Figure 1a, the asymmetric unit of **1** contains two crystallographically independent Zn centers, one $bpta^{4-}$ ligand and one 4,4′-bipy ligand. The Zn1 ion is four coordinated with three carboxylate O atoms from three different $bpta^{4-}$ ligands using monodentate mode and one N atom from the 4,4′-bipy ligand (Zn−O 1.94−1.99 Å; Zn−N 2.02 Å) to show tetrahedral geometry. The Zn2 center is six coordinated in a distorted octahedral geometry with a NO_5 donor set (Zn−O 2.00−2.29 Å; Zn−N 2.05 Å). Four of the oxygen atoms are provided by three carboxylate groups from two $bpta^{4-}$ ligands. One of the carboxylate groups coordinates to the metal center with chelating mode and the other two with monodentate mode. The octahedral coordination environment was completed by one N atom from 4,4′-bipy and one H_2O molecule. Each $bpta^{4-}$ ligand bounds five Zn(II) centers together, and the connection of $bpta^{4-}$ ligands with Zn(II) ions resulted in a complicated two-dimensional (2D) layer (Figure 1b). The adjacent layers are connected through 4,4′-bipy ligands to Zn(II) centers to give rise to the overall three-dimensional (3D) pillar−layer structure (Figure 1c and 1d). Between the layers, there is space occupied by solvent DMF and H_2O molecules. The network contains channels running along the *b* and *c* axis. However, the entrance of channel was blocked and delimited by the biphenyl group of $bpta^{4-}$ ligand from adjacent layers, and the accessible volume in the channels is divided into individual cavities (Figure S1, Supporting Information). After removal of solvent molecules filled in the pore space, the accessible volume is 29.4%, as estimated using the SOLV function of PLATON.[12]

Complex **2** has the same pillar−layer structure as **1** (Figure 2a and 2b). With the 4,4′-bipy ligand replaced by the longer bipyridine ligand azpy, the entrance of the channels is enlarged as well as the interlayer distance. For the channels along the *b* axis, the opening has a size of ~3.6×3.7 Å^2 ($a \times c$) (Figure 2d) and the channels along *c* axis have the dimension ~6.0×3.7 Å^2 ($a \times b$) (Figure 2c), excluding the van der Waals radius of the hydrogen and nitrogen atoms. Also, compared with **1**, the accessible volume in **2** increased to 36.8%.

As no crystal suitable for single-crystal X-ray diffraction measurement was obtained with dipytz used as reactant, we tried to determine the structure of the crystalline product by X-ray powder diffraction spectra (XRPD). As expected, complex **3** should have the same pillar−layer structure as that of **1** and **2**. Then the XRPD of the prepared sample of **3** should indicate a layered structure related to that of **1** and **2**. Indeed, some reflections in its pattern practically matched those of **1** and **2** indexed as (*h*,0,0) (Figure 3). For **1**, the first reflection appeared at $2\theta = 7.820°$, which corresponds to an interlayer distance of 11.30 Å. For **3**, the first reflection appeared at $2\theta = 5.643°$, corresponding to a structural periodicity of 15.64 Å in the crystal

dx.doi.org/10.1021/ic2004485 |*Inorg. Chem.* 2011, 50, 7555–7562

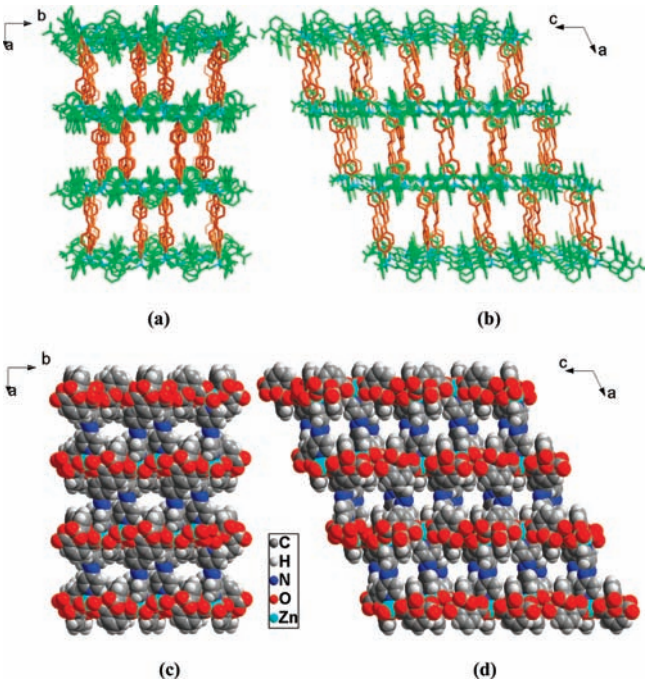

Figure 2. Pillar-layer structure and space-filling views of **2**: (a and c) views along the *c* axis; (b and d) views along the *b* axis.

structure. On the basis of our presumption of the structure of **3**, the interlayer distance should be longer as the layers were separated by the longer pillar dipytz. To verify the presumption, we did a theoretical study of the structure of dipytz and 4,4′-bipy ligands by using density functional theory (DFT) with the Gaussian03 program package.[13] The optimization results at the B3LYP/6-31 g(d)[14] level showed that the distance between the two nitrogen atoms of the two pyridine rings in dipytz and 4,4′-bipy is about 11.16 and 7.14 Å, respectively. The length difference between dipytz and 4,4′-bipy from DFT calculation is 11.16−7.14 = 4.02 Å. This value goes well with the interlayer distance difference calculated from XRPD (15.64−11.30 = 4.34 Å). Also, the only acceptable solution for crystal cell parameters of **3** from XRPD data was found in the monoclinic system with a = 34.45 Å, b = 14.05 Å, c = 18.99 Å, and β = 114.98° (see Supporting Information). This is consistent with the crystal cell parameters of **1** and **2**. Then it could be concluded that complex **3** has the same pillar−layer structure as that of complexes **1** and **2** with dipytz as the pillar ligand. Then the framework component could be assigned as $Zn_4(bpta)_2(dipytz)_2(H_2O)_2$. The solvent molecules in the channels are established to be 1 H_2O and 4 DMF molecules per $Zn_4(bpta)_2(dipytz)_2(H_2O)_2$ unit by elemental analysis.

Structure analysis of complexes **1**−**3** indicated a rule that when H_4bpta was allowed to coordinate with Zn(II) ions in DMF/ethanol solvent, $[Zn_4(bpta)_2(H_2O)_2]$ layer structure is preferred. Furthermore, the layer structure could be expanded into 3D architectures with bipyridine ligands such as 4,4′-bipy, azpy and dipytz as pillars. This synthetic strategy allows a systematic variation of the pillar ligands to achieve open frameworks with tunable window dimensions and pore volume. Also, the well-knit layer could prevent the occurrence of interpenetration when longer pillar ligands are used.

X-ray Power Diffraction. X-ray power diffraction (XRPD) was used to confirm the phase purity of **1**, **2**, and **3** (Figures S3−S5, Supporting Information). The patterns for the as-synthesized bulk products closely match the simulated ones from single-crystal analysis, which are indicative of the pure solid-state phases. The solvent-exchanged and vacuum activated samples are still crystalline, as evidenced by the XRPD patterns, which indicated the good stability of the frameworks after removal of solvent molecules. The shift of several peaks and appearance of a few new peaks is due to distortion of the crystal lattice in response to removal of guest molecules, commonly observed in many other MOFs structures.[1d,15]

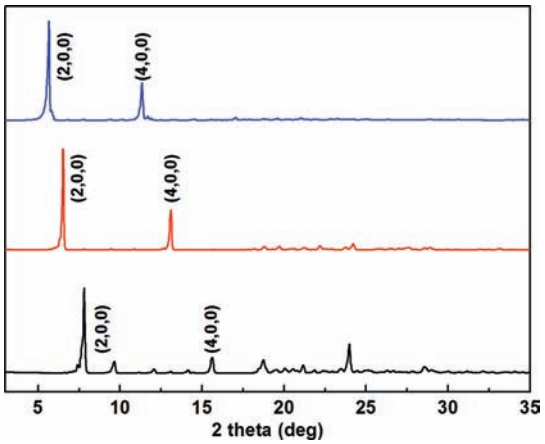

Figure 3. XRPD patterns of **1** (bottom), **2** (middle), and **3** (top) and the assignment of the main reflections.

Thermal Properties. Thermogravimetric analysis (TGA) of **1** (Figure S2a, Supporting Information) showed no weight loss before 178 °C, and then it reveals a weight loss of 8.5% in the temperature range of 178−348 °C. This value is much lower than the calculated value for all three DMF and one H_2O solvent molecules in the cavity (15.9%). Then the loss of weight was attributed to one DMF, one free H_2O molecule, and two coordinated H_2O molecules per formula unit (calcd 8.5%). To fully remove the DMF molecules, we tried to exchange the solvent molecules in the cavities with methanol. However, even after soaking the sample in methanol for 3 days, the TG curve does not show obvious change, which indicated failure of solvent exchange. This is consistent with the crystal structure of **1** where the entrance of cavities is blocked by phenyl rings of H_4bpta ligands.

The TG curve of **2** (Figure S2b, Supporting Information) reveals a weight loss of 12.1% from 52 to 242 °C, in excellent agreement with the weight of two DMF and three water molecules (calcd 12.0%). Similar to **1**, only part of the solvent DMF could be removed from the channels by direct heating the as-made sample. After solvent exchange with methanol, the TG curve showed stepwise loss of weight upon heating. In the temperature range of 36−88 °C, the loss of weight could be attributed to the loss of solvent molecules residing in the open channels. The 2.8% loss of weight between 127 and 184 °C was in agreement with the weight of coordinated H_2O molecules (calcd 2.5%, based on guest free framework in the same state).

For **3** (Figure S2c, Supporting Information), the approximate 15.1% weight loss occurring from 34 to 126 °C could be attributed primarily to release of solvent molecules. In contrast to **1** and **2**, the as-synthesized sample of **3** shows a quick loss of weight at a temperature higher than 163 °C. This might be due to hydrolysis of dipytz with ring opening.[4a] Hydrolysis, however, is

dx.doi.org/10.1021/ic2004485 |*Inorg. Chem.* 2011, 50, 7555–7562

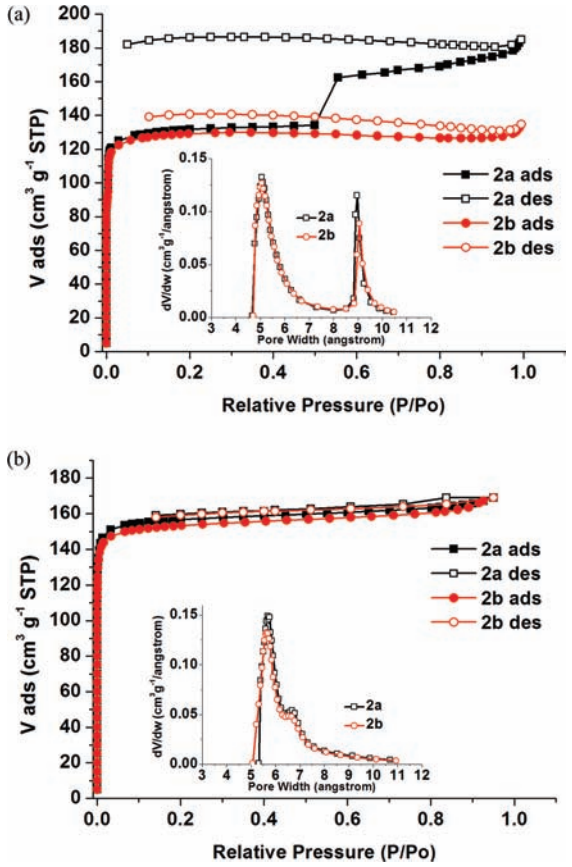

Figure 4. Isothermal adsorption curves of (a) N_2 gas for **2a** (black) and **2b** (red). (Inset) Horvath−Kawazoe pore size distribution plots of **2a** (black) and **2b** (red); (b) O_2 gas for **2a** (black) and **2b** (red). (Inset) Horvath−Kawazoe pore size distribution plots of **2a** (black) and **2b** (red).

prevented after nearly complete guest exchange with methanol. The TG curve of the solvent-exchanged sample is similar to that of **2**. It should be noted that after the loss of coordinated H_2O molecules at 177 °C, the second step of weight loss near 205 °C should be assigned to the smooth decomposition of dipytz to 4-cyanopyridine with the loss of one molecule of nitrogen.[16]

Pore Characterization with N_2 and O_2 Adsorption. To study the porosity of **1**, **2**, and **3**, N_2 and O_2 physisorption measurements were performed at 77 K. For this purpose, the synthesized materials were dried to remove the guest molecules by evacuation under a dynamic vacuum.

To completely remove the solvent in the cavities of **1**, fresh sample was activated at 250 °C to obtain the guest-free sample **1a**. As the TGA result reveals, the solvent was removed completely after activation. However, **1a** adsorbs neither N_2 nor O_2. This is consistent with the crystal structure of **1** in that the small entrance of cavities prevents diffusion of N_2 molecule (kinetic diameter 3.64 Å) and O_2 molecule (kinetic diameter 3.46 Å) within.

On the basis of TGA, activation was performed at 50 and 150 °C to generate materials **2a** with coordinated H_2O and fully dehydrated **2b**, respectively. The nitrogen physisorption measurement reveals that both **2a** and **2b** exhibit type-I isotherms (Figure 4a), indicative of microporous materials. However, the step in the isotherm of **2a** at $P/P_o = 0.5$ as well as the hysteresis of desorption is highly unusual. For **2a**, it has a total pore volume of 0.29 cm^3 g^{-1}. The Langmuir and Brunauer−Emmett−Teller (BET) surface areas are 582 and 440 m^2 g^{-1}, respectively, derived from the adsorption data. Compared with **2a**, **2b** exhibits a similar adsorption behavior before $P/P_o = 0.2$, which results in nearly the same surface area values ($S_{Langmuir}$ = 570 m^2 g^{-1} and S_{BET} = 435 m^2 g^{-1}), and the total pore volume was calculated to be 0.20 cm^3 g^{-1} using the Horvath−Kawazoe model. For both **2a** and **2b**, the fit of the adsorption data to the Horvath−Kawazoe model shows two major pore width distributions. The first range is from 4.5 to 7 Å, which should be attributed to adsorption in the P/P_o range from 6×10^{-7} to 0.003, and the second range is 9−10 Å, corresponding to the step of adsorption at $P/P_o = 0.004$.

To fully understand the stepwise adsorption of nitrogen and the pore structure of **2a** and **2b**, isotherms were recorded using O_2, which has a smaller kinetic diameter than N_2. Unlike the N_2 isotherms, the O_2 isotherms of **2a** and **2b** at 77 K (Figure 4b) show typical one-step adsorption from low pressure to $P/P_o = 1$ with no hysteresis of desorption. Also, the pore width distributions for both **2a** and **2b** are from 5 to 8 Å. Compared with the pore width distribution calculated from N_2 isotherms, the second range at 9−10 Å disappeared while a new peak appeared at ~6.7 Å. A close look at the O_2 isotherms of **2a** and **2b** reveals that the fill of micropore starts at $P/P_o = 3.7 \times 10^{-6}$ for **2b** and $P/P_o = 8.4 \times 10^{-6}$ for **2a** (Figure S6, Supporting Information). The lower start filling pressure in the same situation indicates the micropore in **2b** is narrower than that in **2a**. The difference in porous dimensions might be due to the structure change upon loss of coordinated water molecules (Figure S4, Supporting Information).[17]

The obvious step in the nitrogen isotherm of **2a** at $P/P_o = 0.5$ and hysteresis of desorption is fully repeatable and not simply a consequence of incomplete instrument equilibration. Such stepwise behavior has generally been attributed to multilayer adsorption on energetically homogeneous surfaces, multiple adsorbent−adsorbate interactions that substantially differ in energy, or various structural phase transitions occurring under different adsorbate pressures.[18] For **2a** and **2b**, the stepwise adsorption of nitrogen and two ranges of pore width distribution might be attributed to the pressure-dependent pore-opening/pore-closing process caused by the flexibility of azpy as observed for many flexible framework structures.[19]

Activation of **3** was also performed at 50 and 150 °C based on the TGA result of solvent-exchanged sample. Both **3a** (activated at 50 °C) and **3b** (activated at 150 °C) are microporous materials as the nitrogen and oxygen physisorption measurements reveal type-I isotherms (Figures 5 and S7, Supporting Information). These results proved our prediction of the structure of **3**. Fitting the nitrogen isotherm of **3a** gives the Langmuir and BET surface areas as 529 and 402 m^2 g^{-1} and a total pore volume of 0.19 cm^3 g^{-1} (Horvath−Kawazoe model). For **3b**, the surface area was estimated to be 188 (BET) and 250 m^2 g^{-1} (Langmuir). The total micropore volume was calculated to be 0.10 cm^3 g^{-1} (Horvath−Kawazoe model). As expected, introduction of a longer pillar ligand (dipytz) into the pillar−layer structure should increase the pore volume. The nitrogen and oxygen adsorption results indicate that the aperture of the channel in **3a** and **3b** is indeed enlarged to enable the entrance of N_2 and O_2 molecules compared with **1a**. However, compared with **2a** and **2b**, **3a** does not show increased surface area and pore volume and **3b** even reveals obviously decreased values. These might be attributed to

dx.doi.org/10.1021/ic2004485 |*Inorg. Chem.* 2011, 50, 7555–7562

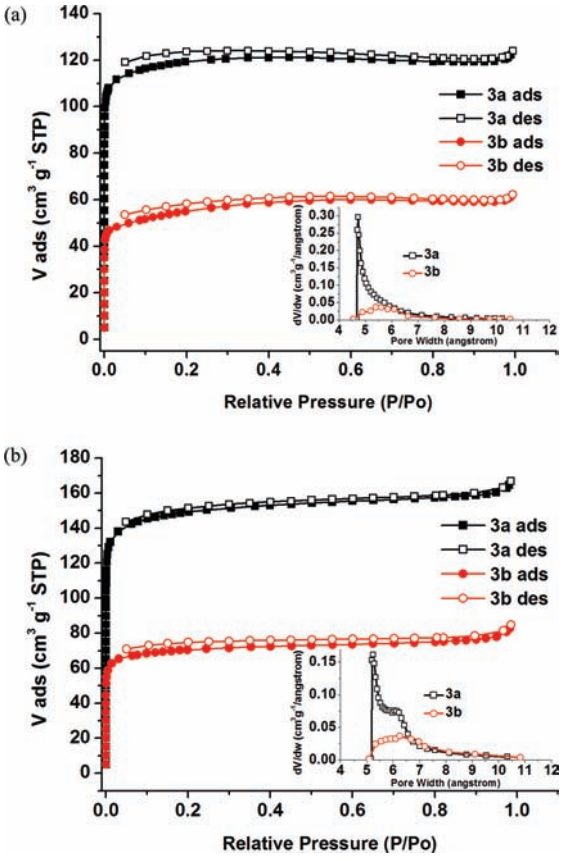

Figure 5. Isothermal adsorption curves of (a) N_2 gas for **3a** (black) and **3b** (red). (Inset) Horvath−Kawazoe pore size distribution plots of **3a** (black) and **3b** (red); (b) O_2 gas for **3a** (black) and **3b** (red). (Inset) Horvath−Kawazoe pore size distribution plots of **3a** (black) and **3b** (red).

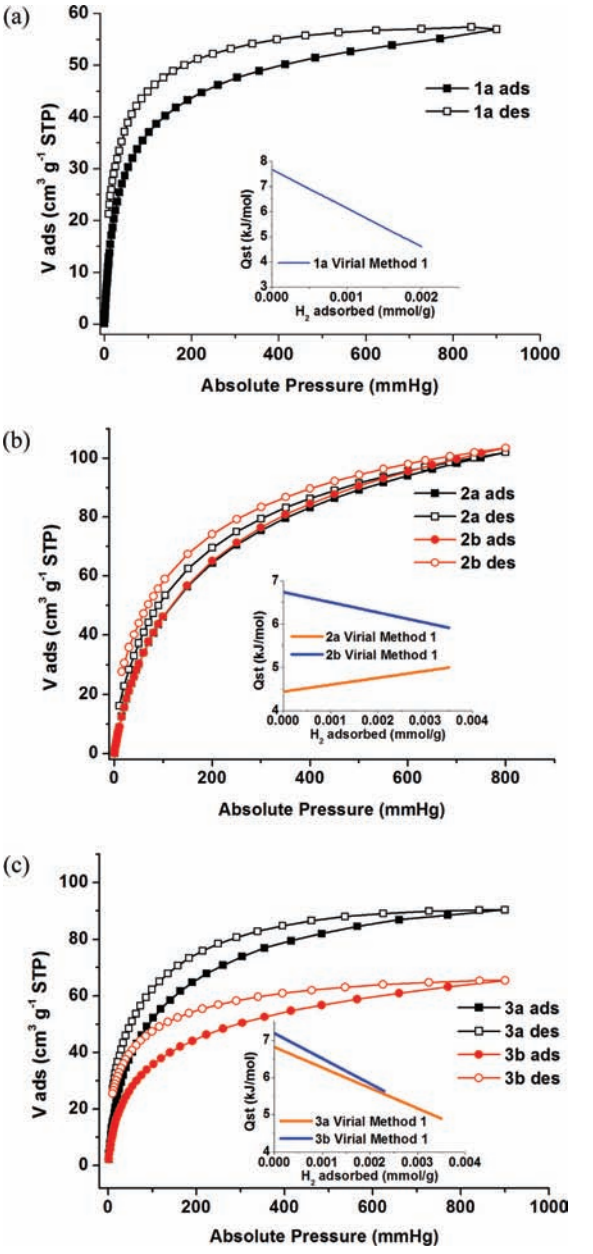

Figure 6. Hydrogen adsorption−desorption isotherms at 77 K and the variation of adsorption enthalpies of hydrogen with uptake of hydrogen: (a) **1a**, (b) **2a** and **2b**, and (c) **3a** and **3b**.

the structure of dipytz ligand. As the structure of **3** is similar to that of **1**, the tetrazine rings in dipytz ligands should reside in the position near the biphenyl group of $bpta^{4-}$ ligands to serve as the gate of the channel. This hypothesis could be proved by the adsorption results as **3a** shows narrower pore width distributions than those of **2a** and **2b**. Though dipytz is a longer pillar than azpy, it is also bulkier; the increased pore volume in **3a** might be counteracted by the synchronously increased volume of the pillar ligand. As a result, the Langmuir and BET surface areas and micropore volume of **3a** are similar to those of **2a** and **2b**, ignoring the excess volume from the flexibility of **2a**. For **3b**, the decreased pore volume and surface area might be due to the structure change upon removal of the coordinated aqua ligands as in the case of **2b** (Figure S5, Supporting Information). To adapt the structure change of the layer structure, the tetrazine ring at the gate position or even the whole dipytz ligand may rotate to minimize the energy of the framework.[19e] These could cause blockage of channels in the framework and a decrease of accessible volume.

Hydrogen Adsorption and Binding Energy. Adsorption of hydrogen by guest-free **1a**, **2a**, **2b**, **3a**, and **3b** was also studied. Though the previous mentioned adsorption isotherms measured at 77 K reveal that **1a** scarcely adsorbs N_2 and O_2 due to its limited pore size, **1a** can absorb a moderate amount of H_2 (57 cm^3 g^{-1}) at 77 K with typical type-I behavior (Figure 6a). Such selective adsorption behavior might be attributed to a size-exclusive effect in which some micropores are only accessible to small gas molecules such as H_2 (kinetic diameter 2.8 Å).[20] The adsorption selectivity of H_2 over N_2 may have applications for hydrogen enrichment of the N_2/H_2 exhaust in ammonia synthesis.[21] To estimate the hydrogen isosteric heats of adsorption (Q_{st}), the hydrogen adsorption data was analyzed using Virial Method 1[22] and Virial Method 2[23] (see Supporting Information for details). Q_{st} for **1a** calculated from the respective adsorption isotherms at 77 and 87 K, employing Virial Method 1 (Figure S8, Supporting Information), are 7.7−4.6 kJ mol^{-1} depending on the degree of H_2 loading, which is in the usual range of the porous MOFs.[24] As the Virial parameters obtained by fitting reveals, the A_1 values are very negative (−1325.1 and −1049.2 g mol^{-1}), which suggests a strong H_2-H_2 interaction inside the framework. These values are in accord with the fact that **1a** has a limited pore size.

dx.doi.org/10.1021/ic2004485 |*Inorg. Chem.* 2011, 50, 7555–7562

The hydrogen adsorption isotherm measured at 77 K reveals an uptake of 102 $cm^3 g^{-1}$ at 800 mmHg for **2a** (Figure 6b). Similarly, the fully dehydrated **2b** affords an uptake of 103 $cm^3 g^{-1}$ at 800 mmHg. Furthermore, the affinity of hydrogen for the frameworks of **2a** and **2b** was probed by extracting isosteric adsorption enthalpies from hydrogen adsorption data measured at 77 and 87 K. These two compounds show initial adsorption enthalpies of 4.4 and 6.7 kJ mol^{-1}, respectively. It should be noted that the Q_{st} values for **2a** obtained using Virial Method 1 show an unusual increased trend with the increasing of H_2 uptake. This could be attributed to the more negative A_1 value for 87 K (-448.8 g mol^{-1}) than that of 77 K (-420.1 g mol^{-1}), which indicates a stronger H_2-H_2 interaction at higher temperature. Also, compared with the A_1 values for **2b** (-401.2 g mol^{-1} at 77 K and -358.6 g mol^{-1} at 87 K), the values for **2a** are more negative at both temperatures. The stronger H_2-H_2 interaction inside the framework of **2a** might be due to its flexible nature. As the framework could expand or shrink depending on the uptake of gases, the interaction between gas molecules in the framework is increased.[25] Furthermore, the stronger H_2-H_2 interaction in the **2a** framework at higher temperature could be explained as the flexibility of the framework is increased at higher temperature. On the other hand, the much higher Q_{st} value attained by **2b** could potentially be a consequence of the vacant metal coordination sites from the loss of coordinated H_2O molecules associated with the presence of narrower pore sequence to the change of structure upon high-temperature activation.[3b,26]

For **3a** and **3b**, the hydrogen sorption isotherms recorded at 77 K under normal pressure show type-I behavior (Figure 6c). The maximum hydrogen uptake of **3a** at 77 K is about 90 $cm^3 g^{-1}$, and the uptake of **3b** is about 65 $cm^3 g^{-1}$ under the same conditions. To determine the hydrogen affinity of **3a** and **3b**, H_2 adsorption isotherms at 87 K were also collected to calculate the heat of adsorption. At low coverage, **3a** and **3b** exhibit Q_{st} of 6.8 and 7.2 kJ mol^{-1} (Virial Method 1), respectively. Compared to the A_0 values for **3a** (-14.0 ln (mol g^{-1} Pa^{-1}))/**3b** (-14.2 ln (mol g^{-1} Pa^{-1})) and **2a** (-14.8 ln (mol g^{-1} Pa^{-1}))/**2b** (-14.9 ln (mol g^{-1} Pa^{-1})), the less negative values for **3a** and **3b** indicate a stronger H_2–framework interaction. According to the pore structure, we consider that the stronger H_2–framework interaction can be mainly attributed to the tetrazine rings decorated pores. It has been reported that the aromatic rings in microporous aromatic-rich MOFs can strengthen the interactions of H_2 molecules with the framework.[27] Compared with the aromatic ring, the tetrazine ring contains more electrons to form an electron-rich conjugated π system; thus, the interaction between H_2 and the tetrazine ring should be stronger than the interaction between H_2 and the aromatic ring. In addition, the A_1 values for **3a** (-687.4 and -589.0 g mol^{-1}) and **3b** (-1080.1 and -959.1 g mol^{-1}) are more negative than that for **2a** and **2b**. Considering the pore structure of these compounds and the higher initial Q_{st} values of **3a** and **3b**, it could be concluded that the smaller size of the tetrazine ring decorated inner surface can overlap the potential energy fields of the pore walls to enhance the H_2 binding energy.[28]

CONCLUSION

We systemically synthesized and characterized a series of pillar–layer structure porous MOFs in which $[Zn_4(bpta)_2(H_2O)_2]$ layers are connected by length-controllable bipyridine pillars. The synthetic strategy allows a systematic variation of the pillar to construct a series of open frameworks with similar structure. Pore volume and window size could be adjusted by selection of pillar ligands, and the resulted three MOFs show different gas adsorption properties depending on their pore structures. In addition, hydrogen adsorption properties of the resulted MOFs were studied. Investigation of this pillar–layer system provides a nice example of controllable construction of porous MOFs, and utilization of longer and bulky pillars is expected to be more profitable for gas storage.

ASSOCIATED CONTENT

Supporting Information. X-ray crystallographic files in CIF format for **1** and **2**, TGA curves, XRPD patterns, and some graphics. This material is available free of charge via the Internet at http://pubs.acs.org.

AUTHOR INFORMATION

Corresponding Author
*E-mail: buxh@nankai.edu.cn.

ACKNOWLEDGMENT

We are thankful for the financial support from the 973 Program of China (2007CB815305), NSFC (21031002 and 51073079), and Natural Science Fund of Tianjin, China (10JCZDJC22100).

REFERENCES

(1) (a) Yaghi, O. M.; O'Keeffe, M.; Ockwig, N. W.; Chae, H. K.; Eddaoudi, M.; Kim, J. *Nature* **2003**, *423*, 705.(b) Uemura, T.; Kitagawa, S. Controlled Polymerization by Incarceration of Monomers in Nanochannels. In *Functional Metal-Organic Frameworks: Gas Storage, Separation and Catalysis*; Springer-Verlag Berlin: Berlin, 2010; Vol. 293, pp 155. (c) Férey, G. *Chem Soc Rev* **2008**, *37*, 191. (d) Mulfort, K. L.; Farha, O. K.; Malliakas, C. D.; Kanatzidis, M. G.; Hupp, J. T. *Chem.-Eur. J* **2010**, *16*, 276. (e) Holliday, B. J.; Mirkin, C. A. *Angew Chem Int Edit* **2001**, *40*, 2022. (f) Yang, S. H.; Lin, X.; Dailly, A.; Blake, A. J.; Hubberstey, P.; Champness, N. R.; Schröder, M. *Chem.—Eur. J.* **2009**, *15*, 4829. (g) Li, Z. Y.; Zhu, G. S.; Lu, G. Q.; Qiu, S. L.; Yao, X. D. *J. Am. Chem. Soc.* **2010**, *132*, 1490. (h) Lin, J. B.; Zhang, J. P.; Chen, X. M. *J. Am. Chem. Soc.* **2010**, *132*, 6654. (i) Li, J. R.; Tao, Y.; Yu, Q.; Bu, X. H.; Sakamoto, H.; Kitagawa, S. *Chem.—Eur. J* **2008**, *14*, 2771.

(2) (a) Perry, J. J.; Perman, J. A.; Zaworotko, M. J. *Chem. Soc. Rev.* **2009**, *38*, 1400. (b) Kim, J.; Chen, B. L.; Reineke, T. M.; Li, H. L.; Eddaoudi, M.; Moler, D. B.; O'Keeffe, M.; Yaghi, O. M. *J. Am. Chem. Soc.* **2001**, *123*, 8239. (c) Sakamoto, H.; Kitaura, R.; Matsuda, R.; Kitagawa, S.; Kubota, Y.; Takata, M. *Chem. Lett.* **2010**, *39*, 218. (d) Férey, G.; Mellot-Draznieks, C.; Serre, C.; Millange, F.; Dutour, J.; Surble, S.; Margiolaki, I. *Science* **2005**, *309*, 2040. (e) Wang, X. L.; Qin, C.; Wu, S. X.; Shao, K. Z.; Lan, Y. Q.; Wang, S.; Zhu, D. X.; Su, Z. M.; Wang, E. B. *Angew. Chem., Int. Ed.* **2009**, *48*, 5291.

(3) (a) Barrio, J. P.; Rebilly, J. N.; Carter, B.; Bradshaw, D.; Bacsa, J.; Ganin, A. Y.; Park, H.; Trewin, A.; Vaidhyanathan, R.; Cooper, A. I.; Warren, J. E.; Rosseinsky, M. J. *Chem.—Eur. J* **2008**, *14*, 4521. (b) Chen, B. L.; Xiang, S. C.; Qian, G. D. *Acc. Chem. Res.* **2010**, *43*, 1115. (c) Yao, Q. X.; Pan, L.; Jin, X. H.; Li, J.; Ju, Z. F.; Zhang, J. *Chem.—Eur. J.* **2009**, *15*, 11890. (d) Chen, B.; Zhao, X.; Putkham, A.; Hong, K.; Lobkovsky, E. B.; Hurtado, E. J.; Fletcher, A. J.; Thomas, K. M. *J. Am. Chem. Soc.* **2008**, *130*, 6411.

(4) (a) Vagin, S. I.; Ott, A. K.; Hoffmann, S. D.; Lanzinger, D.; Rieger, B. *Chem.—Eur. J* **2009**, *15*, 5845. (b) Lan, A. J.; Li, K. H.; Wu, H. H.; Kong, L. Z.; Nijem, N.; Olson, D. H.; Emge, T. J.; Chabal, Y. J.; Langreth, D. C.; Hong, M. C.; Li, J. *Inorg. Chem.* **2009**, *48*, 7165.

(5) Chang, Z.; Zhang, A. S.; Hu, T. L.; Bu, X. H. *Cryst. Growth Des.* **2009**, *9*, 4840.
(6) (a) Davies, R. P.; Less, R.; Lickiss, P. D.; Robertson, K.; White, A. J. P. *Cryst. Growth Des.* **2010**, *10*, 4571. (b) Liu, D. M.; Xie, Z. G.; Ma, L. Q.; Lin, W. B. *Inorg. Chem.* **2010**, *49*, 9107.
(7) Pryor, K. E.; Shipps, G. W.; Skyler, D. A.; Rebek, J. *Tetrahedron* **1998**, *54*, 4107.
(8) Schalley, C. A.; Muller, T.; Linnartz, P.; Witt, M.; Schafer, M.; Lutzen, A. *Chem.—Eur. J.* **2002**, *8*, 3538.
(9) Dinolfo, P. H.; Williams, M. E.; Stern, C. L.; Hupp, J. T. *J. Am. Chem. Soc.* **2004**, *126*, 12989.
(10) *SAINT Software Reference Manual*; Bruker AXS: Madison, WI, 1998.
(11) Sheldrick, G. M. *SHELXTL NT*, Version 5.1 (Program for Solution and Refinement of Crystal Structures); University of Göttingen: Göttingen, Germany, 1997.
(12) Spek, A. L. *J. Appl. Crystallogr.* **2003**, *36*, 7.
(13) Frisch, M. J. *Gaussian 03*, Revision E.01; Gaussian, Inc.: Wallingford, CT, 2004.
(14) (a) Stephens, P. J.; Devlin, F. J.; Chabalowski, C. F.; Frisch, M. J. *J. Phys. Chem.* **1994**, *98*, 11623. (b) Becke, A. D. *J. Chem. Phys.* **1993**, *98*, 5648.
(15) Chen, B.; Ma, S.; Zapata, F.; Fronczek, F. R.; Lobkovsky, E. B.; Zhou, H.-C. *Inorg. Chem.* **2007**, *46*, 1233.
(16) (a) Ramirez, F.; Chen, E. H.; Dershowitz, S. *J. Am. Chem. Soc.* **1959**, *81*, 4342. (b) Lee, J. Y.; Roberts, J. M.; Farha, O. K.; Sarjeant, A. A.; Scheidt, K. A.; Hupp, J. T. *Inorg. Chem.* **2009**, *48*, 9971.
(17) Ghosh, S. K.; Zhang, J. P.; Kitagawa, S. *Angew. Chem., Int. Ed.* **2007**, *46*, 7965.
(18) Choi, H. J.; Dinca, M.; Long, J. R. *J. Am. Chem. Soc.* **2008**, *130*, 7848.
(19) (a) Maji, T. K.; Mostafa, G.; Matsuda, R.; Kitagawa, S. *J. Am. Chem. Soc.* **2005**, *127*, 17152. (b) Kondo, A.; Noguchi, H.; Carlucci, L.; Proserpio, D. M.; Ciani, G.; Kajiro, H.; Ohba, T.; Kanoh, H.; Kaneko, K. *J. Am. Chem. Soc.* **2007**, *129*, 12362. (c) Cussen, E. J.; Claridge, J. B.; Rosseinsky, M. J.; Kepert, C. J. *J. Am. Chem. Soc.* **2002**, *124*, 9574. (d) Llewellyn, P. L.; Bourrelly, S.; Serre, C.; Filinchuk, Y.; Ferey, G. *Angew. Chem., Int. Ed.* **2006**, *45*, 7751. (e) Culp, J. T.; Smith, M. R.; Bittner, E.; Bockrath, B. *J. Am. Chem. Soc.* **2008**, *130*, 12427.
(20) Xue, M.; Zhang, Z.; Xiang, S.; Jin, Z.; Liang, C.; Zhu, G.-S.; Qiu, S.-L.; Chen, B. *J. Mater. Chem.* **2010**, *20*, 3984.
(21) (a) Zou, Y.; Hong, S.; Park, M.; Chun, H.; Lah, M. S. *Chem. Commun.* **2007**, 5182. (b) Ma, S. Q.; Wang, X. S.; Collier, C. D.; Manis, E. S.; Zhou, H. C. *Inorg. Chem.* **2007**, *46*, 8499. (c) Xue, M.; Ma, S. Q.; Jin, Z.; Schaffino, R. M.; Zhu, G. S.; Lobkovsky, E. B.; Qiu, S. L.; Chen, B. L. *Inorg. Chem.* **2008**, *47*, 6825. (d) Dinca, M.; Long, J. R. *J. Am. Chem. Soc.* **2005**, *127*, 9376. (e) Dybtsev, D. N.; Chun, H.; Yoon, S. H.; Kim, D.; Kim, K. *J. Am. Chem. Soc.* **2004**, *126*, 32. (f) Navarro, J. A. R.; Barea, E.; Rodriguez-Dieguez, A.; Salas, J. M.; Ania, C. O.; Parra, J. B.; Masciocchi, N.; Galli, S.; Sironi, A. *J. Am. Chem. Soc.* **2008**, *130*, 3978.
(22) (a) Cole, J. H.; Everett, D. H.; Marshall, C. T.; Paniego, A. R.; Powl, J. C.; Rodriguez-Reinoso, F. *J. Chem. Soc., Faraday Trans. 1: Phys. Chem. Condens. Phases* **1974**, *70*, 2154. (b) O'Koye, I. P.; Benham, M.; Thomas, K. M. *Langmuir* **1997**, *13*, 4054. (c) Reid, C. R.; O'Koy, I. P.; Thomas, K. M. *Langmuir* **1998**, *14*, 2415. (d) Reid, C. R.; Thomas, K. M. *Langmuir* **1999**, *15*, 3206.
(23) (a) Czepirski, L.; JagieLlo, J. *Chem. Eng. Sci.* **1989**, *44*, 797. (b) Ansón, A.; Jagiello, J.; Parra, J. B.; Sanjuán, M. L.; Benito, A. M.; Maser, W. K.; Martínez, M. T. *J. Phys. Chem. B* **2004**, *108*, 15820. (c) Reid, C. R.; Thomas, K. M. *J. Phys. Chem. B* **2001**, *105*, 10619.
(24) (a) Schmitz, B.; Muller, U.; Trukhan, N.; Schubert, M.; Férey, G.; Hirscher, M. *ChemPhysChem* **2008**, *9*, 2181. (b) Dinca, M.; Dailly, A.; Tsay, C.; Long, J. R. *Inorg. Chem.* **2008**, *47*, 11. (c) Guo, Z. Y.; Li, G. H.; Zhou, L.; Su, S. Q.; Lei, Y. Q.; Dang, S.; Zhang, H. J. *Inorg. Chem.* **2009**, *48*, 8069.
(25) (a) Matsuda, R.; Kitaura, R.; Kubota, Y.; Kobayashi, T. C.; Takata, M.; Kitagawa, S. *Microporous Mesoporous Mater.* **2010**, *129*, 296. (b) Uemura, K.; Matsuda, R.; Kitagawa, S. *J. Solid State Chem.* **2005**, *178*, 2420.
(26) Luo, J. H.; Xu, H. W.; Liu, Y.; Zhao, Y. S.; Daemen, L. L.; Brown, C.; Timofeeva, T. V.; Ma, S. Q.; Zhou, H. C. *J. Am. Chem. Soc.* **2008**, *130*, 9626.
(27) (a) Nechaev, Y. S.; Alexeeva, O. K. *Int. J. Hydrogen Energy* **2003**, *28*, 1433. (b) Li, J.; Furuta, T.; Goto, H.; Ohashi, T.; Fujiwara, Y.; Yip, S. *J. Chem. Phys.* **2003**, *119*, 2376. (c) Hubner, O.; Gloss, A.; Fichtner, M.; Klopper, W. *J. Phys. Chem. A* **2004**, *108*, 3019. (d) Frost, H.; Duren, T.; Snurr, R. Q. *J. Phys. Chem. B* **2006**, *110*, 9565. (e) Belof, J. L.; Stern, A. C.; Eddaoudi, M.; Space, B. *J. Am. Chem. Soc.* **2007**, *129*, 15202.
(28) Zhong, D. C.; Lin, J. B.; Lu, W. G.; Jiang, L.; Lu, T. B. *Inorg. Chem.* **2009**, *48*, 8656.